METHODS AND APPLICATIONS OF ANALYSIS.
Vol. 20, No. 4, pp. 405–424, December 2013

006

WHEN EULER-POISSON-DARBOUX MEETS PAINLEVÉ AND BRATU: ON THE NUMERICAL SOLUTION OF NONLINEAR WAVE EQUATIONS*

ROLAND GLOWINSKI† AND ANNALISA QUAINI‡

Dedicated to Stanley Osher on the occasion of his 70^{th} anniversary

Abstract. The main goal of this article is to extend to Euler-Poisson-Darboux nonlinear wave equations the computational methods we employed in a previous work to solve a nonlinear equation coupling the classical wave operator with the nonlinear forcing term of the Painlevé I ordinary differential equation. In order to handle the extra (dissipative) term with singular coefficient encountered in the Euler-Poisson-Darboux equations, we advocate a five stage symmetrized operator-splitting scheme for the time-discretization. This scheme, combined with a finite element space discretization and adaptive time-stepping to monitor possible blow-up of the solution, provides a robust and accurate solution methodology, as shown by the results of the numerical experiments reported here. The nonlinearities we have considered are those encountered in the Painlevé I and II equations (and close variants of them), and the exponential one encountered in the celebrated Bratu problem.

Key words. Euler-Poisson-Darboux nonlinear wave equations, Painlevé equations, Bratu problem, blow-up solutions, operator-splitting.

AMS subject classifications. 35L70, 65N30.

1. Introduction. In a recent article (ref. [1]) we discussed the numerical solution of the following nonlinear wave equation:

$$\frac{\partial^2 u}{\partial t^2} - c^2\nabla^2 u = 6u^2 + t \quad \text{in } \Omega \times (0, T_{max}), \tag{1}$$

completed by boundary and initial conditions. The solution method discussed in [1] relies on a three-stage symmetrized operator-splitting time discretization scheme of the Strang's type [2], which allows the uncoupled treatment of the differential operator $-c^2\nabla^2$ and of the nonlinear forcing term (originating from the Painlevé I ordinary differential equation) in (1). Combined with an appropriate finite element space discretization, and an adaptive time-stepping method to control possible finite time blow-up of the solution, the above splitting scheme provides a robust and accurate solution method, as shown by the numerical results reported in [1].

Our goal here is to extend the methodology discussed in [1] to achieve the numerical solution of *nonlinear wave equations* of the *Euler-Poisson-Darboux* type, namely:

$$\frac{\partial^2 u}{\partial t^2} + \frac{k}{t}\frac{\partial u}{\partial t} - c^2\nabla^2 u = f(u,t) \quad \text{in } \Omega \in (0, T_{\max}), \tag{2}$$

where

- Ω is a bounded domain of $\mathbb{R}^d$ $(d \geq 1)$.
- $k > 0$.

*Received December 17, 2012; accepted for publication May 2, 2013.

†Department of Mathematics, University of Houston, 4800 Calhoun Rd, Houston (TX) 77204, USA (roland@math.uh.edu); and Laboratoire Jacques-Louis Lions, Université Pierre et Marie Curie - 4, place Jussieu - 75252, Paris CEDEX 05, France.

‡Department of Mathematics, University of Houston, 4800 Calhoun Rd, Houston (TX) 77204, USA (quaini@math.uh.edu).

- f is a two-variable function, possibly complex-valued.

Equation (2) has to be completed by boundary and initial conditions. Concerning the initial conditions, we assume using standard notation that:

$$u(0) = u_0, \quad \frac{\partial u}{\partial t}(0) = u_1. \tag{3}$$

On the boundary, we will impose a homogeneous Dirichlet condition for simplicity

$$u = 0 \quad \text{on } \partial\Omega \times (0, T_{\max}). \tag{4}$$

The extension to mixed Dirichlet-Sommerfeld conditions:

$$u = 0 \text{ on } \Gamma_0 \times (0, T_{\max}), \frac{1}{c}\frac{\partial u}{\partial t} + \frac{\partial u}{\partial n} = 0 \text{ on } \Gamma_1 \times (0, T_{\max}), \tag{5}$$

with $\Gamma_0 \cap \Gamma_1 = \emptyset$ and $\Gamma_0 \cup \Gamma_1 = \partial\Omega$, is straightforward (see [1]).

The existence of solutions to nonlinear wave equations very close to (2) has been investigated by J.B. Keller in [3], assuming that $u_1 = 0$ in (3). In this work, we would like to include also the case with $u_1 \neq 0$. Thus, instead of (2), we will consider

$$\frac{\partial^2 u}{\partial t^2} + \frac{k}{\epsilon + t}\frac{\partial u}{\partial t} - c^2\nabla^2 u = f(u, t) \quad \text{in } \Omega \in (0, T_{\max}), \tag{6}$$

with $\epsilon \geq 0$.

In order to solve (6), we advocate a five-stage operator splitting scheme of the Strang symmetric type, close (in some sense) to the scheme discussed in [4] for the solution of a nonlinear integro-differential equation. The scheme we are going to use is also close to the three-stage scheme used in [1] for the solution of a non-damped version of problem (6), that is problem (1). Actually, in the present article, in addition to the nonlinear forcing occurring in (1), that is $f(u, t) = 6u^2 + t$, we are going to consider the case $f(u, t) = 2u^3 + tu + \gamma$ (with $\gamma \in \mathbb{C}$), which is the nonlinear term of the Painlevé II equation, and $f(u, t) = \lambda e^u$, which is the nonlinear term of the celebrated Bratu equation $-\nabla^2 u = \lambda e^u$.

REMARK 1.1. *The analysis of quasilinear parabolic equations with blow-up has motivated a substantial number of publications (see, e.g., [6] and references therein). Similarly, much literature has been devoted to the analysis and numerical analysis of nonlinear Schrödinger equations with blow-up (see, e.g., [7] and references therein). Concerning the Euler-Poisson-Darboux problem considered in this article, J.B. Keller has proved blow-up in finite time properties and has provided an estimate of the blow-up time (see [3] for details). Albeit bearing the name of some of the most famous mathematicians of all times, the Euler-Poisson-Darboux problem has not attracted much attention from a numerical standpoint, a notable exception being [5] which focuses on linear cases. We are not aware of any publication addressing the numerical solution of the nonlinear Euler-Poisson-Darboux problem.*

We will start our discussion with the solution of problem (6),(3),(4).

2. Numerical solution of the nonlinear wave problem (6),(3),(4). First, we introduce $p = \dfrac{\partial u}{\partial t}$ to reformulate the above problem as a *first order* in time system

on which we will apply the Strang's symmetrized scheme repeatedly. This first order system reads as:

$$
(7)\qquad \begin{cases} \dfrac{\partial u}{\partial t} - p = 0 \quad \text{on } \Omega \times (0, T_{\max}), \\ \dfrac{\partial p}{\partial t} + \dfrac{k}{\epsilon + t} p - c^2 \nabla^2 u = f(u,t) \quad \text{in } \Omega \times (0, T_{max}), \\ u = 0 \quad \text{on } \partial\Omega \times (0, T_{max}), \\ u(0) = u_0, p(0) = u_1. \end{cases}
$$

Let Δt be a time-step (fixed, for simplicity) and let us denote $(n+\theta)\Delta t$ by $t^{n+\theta}$. Let us consider next $\alpha, \beta \in (0,1)$, such that $\alpha + \beta = 1$. Inspired by the three-operator situation discussed in [1], we suggest the following five-stage operator splitting scheme for the time-discretization of problem (7):

- Step 0: Set

$$
(8)\qquad u^0 = u_0,\ p^0 = u_1.
$$

For $n \geq 0$, $\{u^n, p^n\}$ being known, compute $\{u^{n+1}, p^{n+1}\}$ as follows:

- Step 1: Set $u^{n+1/5} = u(t^{n+1/2})$, $p^{n+1/5} = p(t^{n+1/2})$, $\{u, p\}$ being the solution of

$$
(9)\qquad \begin{cases} \dfrac{\partial u}{\partial t} - \alpha p = 0 \text{ in } \Omega \times (t^n, t^{n+1/2}), \\ \dfrac{\partial p}{\partial t} = f(u,t) \text{ in } \Omega \times (t^n, t^{n+1/2}), \\ u(t^n) = u^n, p(t^n) = p^n. \end{cases}
$$

- Step 2: Set $u^{n+2/5} = u\left(\dfrac{\Delta t}{2}\right)$, $p^{n+2/5} = p\left(\dfrac{\Delta t}{2}\right)$, $\{u, p\}$ being the solution of

$$
(10)\qquad \begin{cases} \dfrac{\partial u}{\partial t} = 0 \text{ in } \Omega \times \left(0, \dfrac{\Delta t}{2}\right), \\ \dfrac{\partial p}{\partial t} + \dfrac{k}{\epsilon + t^{n+1/2}} p = 0 \text{ in } \Omega \times \left(0, \dfrac{\Delta t}{2}\right), \\ u(0) = u^{n+1/5}, p(0) = p^{n+1/5}. \end{cases}
$$

- Step 3: Set $u^{n+3/5} = u(\Delta t)$, $p^{n+3/5} = p(\Delta t)$, $\{u, p\}$ being the solution of

$$
(11)\qquad \begin{cases} \dfrac{\partial u}{\partial t} - \beta p = 0 \text{ in } \Omega \times (0, \Delta t), \\ \dfrac{\partial p}{\partial t} - c^2 \nabla^2 u = 0 \text{ in } \Omega \times (0, \Delta t), \\ u = 0 \text{ on } \partial\Omega \times (0, \Delta t), \\ u(0) = u^{n+2/5}, p(0) = p^{n+2/5}. \end{cases}
$$

- Step 4: Set $u^{n+4/5} = u(\Delta t)$, $p^{n+4/5} = p(\Delta t)$, $\{u, p\}$ being the solution of

$$\begin{cases} \dfrac{\partial u}{\partial t} = 0 \text{ in } \Omega \times \left(\dfrac{\Delta t}{2}, \Delta t\right), \\ \dfrac{\partial p}{\partial t} + \dfrac{k}{\epsilon + t^{n+1/2}} p = 0 \text{ in } \Omega \times \left(\dfrac{\Delta t}{2}, \Delta t\right), \\ u\left(\dfrac{\Delta t}{2}\right) = u^{n+3/5}, p\left(\dfrac{\Delta t}{2}\right) = p^{n+3/5}. \end{cases} \tag{12}$$

- Step 5: Set $u^{n+1} = u(t^{n+1})$, $p^{n+1} = p(t^{n+1})$, $\{u, p\}$ being the solution of

$$\begin{cases} \dfrac{\partial u}{\partial t} - \alpha p = 0 \text{ in } \Omega \times (t^{n+1/2}, t^{n+1}), \\ \dfrac{\partial p}{\partial t} = f(u, t) \text{ in } \Omega \times (t^{n+1/2}, t^{n+1}), \\ u(t^{n+1/2}) = u^{n+4/5}, p(t^{n+1/2}) = p^{n+4/5}. \end{cases} \tag{13}$$

By partial elimination of p, (8)-(13) reduces to:

- Step 0 as in (8).

For $n \geq 0$, $\{u^n, p^n\}$ being known, compute $\{u^{n+1}, p^{n+1}\}$ as follows:

- Step 1: Set $u^{n+1/5} = u(t^{n+1/2})$, $p^{n+1/5} = \dfrac{1}{\alpha}\dfrac{\partial u}{\partial t}(t^{n+1/2})$, u being the solution of

$$\begin{cases} \dfrac{\partial^2 u}{\partial t^2} = \alpha f(u, t) \text{ in } \Omega \times (t^n, t^{n+1/2}), \\ u(t^n) = u^n, \dfrac{\partial u}{\partial t}(t^n) = \alpha p^n. \end{cases} \tag{14}$$

- Step 2: Set $u^{n+2/5} = u^{n+1/5}$, $p^{n+2/5} = p\left(\dfrac{\Delta t}{2}\right)$, p being the solution of

$$\begin{cases} \dfrac{\partial p}{\partial t} + \dfrac{k}{\epsilon + t^{n+1/2}} p = 0 \text{ in } \Omega \times \left(0, \dfrac{\Delta t}{2}\right), \\ p(0) = p^{n+1/5}. \end{cases} \tag{15}$$

- Step 3: Set $u^{n+3/5} = u(\Delta t)$, $p^{n+3/5} = \dfrac{1}{\beta}\dfrac{\partial u}{\partial t}(\Delta t)$, u being the solution of

$$\begin{cases} \dfrac{\partial^2 u}{\partial t^2} - \beta c^2 \nabla^2 u = 0 \text{ in } \Omega \times (0, \Delta t), \\ u = 0 \text{ on } \partial\Omega \times (0, \Delta t), \\ u(0) = u^{n+2/5}, \dfrac{\partial u}{\partial t}(0) = \beta p^{n+2/5}. \end{cases} \tag{16}$$

- Step 4: Set $u^{n+4/5} = u^{n+3/5}$, $p^{n+4/5} = p\,(\Delta t)$, p being the solution of

$$\left\{ \begin{array}{l} \dfrac{\partial p}{\partial t} + \dfrac{k}{\epsilon + t^{n+1/2}} p = 0 \text{ in } \Omega \times \left(\dfrac{\Delta t}{2}, \Delta t \right), \\ \\ p\left(\dfrac{\Delta t}{2} \right) = p^{n+3/5}. \end{array} \right. \tag{17}$$

- Step 5: Set $u^{n+1} = u(t^{n+1})$, $p^{n+1} = \dfrac{1}{\alpha} \dfrac{\partial u}{\partial t}(t^{n+1})$, u being the solution of

$$\left\{ \begin{array}{l} \dfrac{\partial^2 u}{\partial t^2} = \alpha f(u,t) \text{ in } \Omega \times (t^{n+1/2}, t^{n+1}), \\ \\ u(t^{n+1/2}) = u^{n+4/5}, \dfrac{\partial u}{\partial t}(t^{n+1/2}) = \alpha p^{n+4/5}. \end{array} \right. \tag{18}$$

Sub-problem (16), which is an initial boundary value problem for a linear wave equation, is a very classical problem. For its space discretization, we will use (as in [1])) finite element spaces consisting of globally continuous functions, piecewise linear over a triangulation of Ω. In the particular case where Ω is a rectangle, as in Sec. 4, we recommend using uniform triangulations. For the time discretization, we will adopt a centered second order finite difference scheme; see [1] for details.

The numerical solution of the initial value sub-problems (14) and (18) will be discussed in the next section, generalizing what we already presented in [1].

The sub-problems (15) and (17) are new in the context of these nonlinear wave problems. Fortunately, they have closed-form solutions given by:

$$p^{n+2/5} = e^{-\frac{k\Delta t}{2(\epsilon + t^{n+1/2})}} p^{n+1/5}, \quad p^{n+4/5} = e^{-\frac{k\Delta t}{2(\epsilon + t^{n+1/2})}} p^{n+3/5}, \tag{19}$$

respectively.

3. On the numerical solution of the sub-initial value problems (14) and (18). From $n = 0$ until blow-up, we have to solve the initial value sub-problems (14) and (18) for almost every point of Ω. Each of these sub-problem is of the following type:

$$\left\{ \begin{array}{l} \dfrac{d^2\psi}{dt^2} = \alpha f(\psi, t) \text{ on } (t_0, t_f), \\ \\ \psi(t_0) = \psi_0, \dfrac{d\psi}{dt}(t_0) = \psi_1. \end{array} \right. \tag{20}$$

A time-stepping scheme for the discretization of (20), with automatic adjustment of the time-step, will be discussed in the following section.

3.1. A centered scheme for the time discretization of problem (20). Let M be a positive integer (> 2 in practice). With M, we associate a time discretization step $\sigma = (t_f - t_0)/M$. For the time discretization of the initial value problem (20) we suggest the following scheme: Set

$$\psi^0 = \psi_0, \ \psi^1 - \psi^{-1} = 2\sigma\psi_1,$$

then for $m = 0, ..., M$, compute ψ^{m+1} from ψ^{m-1} and ψ^m via

$$\psi^{m+1} + \psi^{m-1} - 2\psi^m = \alpha\sigma^2 f(\psi^m, t^m), \tag{21}$$

with $t^m = t^0 + m\sigma$.

Considering the possible blowing-up properties of the solutions of the nonlinear wave problems (6),(3),(4), we expect that at one point in time the solution of problem (20) may start growing very quickly before becoming infinite. In order to track such a behavior we have to decrease σ in (21), until the solution reaches some threshold at which we decide to stop computing. A practical method for the adaptation of the time-step σ is described below.

3.2. On the dynamical adaptation of the time-step σ. The starting point of our adaptive strategy will be the following observation: if ψ is the solution of (20), at a time t before blow-up and for σ sufficiently small we have (*Taylor's expansion*):

$$\begin{aligned}\psi(t+\sigma) =& \psi(t) + \sigma\dot{\psi}(t) + \frac{\sigma^2}{2}\ddot{\psi}(t) + \frac{\sigma^3}{6}\dddot{\psi}(t+\theta\sigma)\\ =& \psi(t) + \sigma\dot{\psi}(t) + \frac{\sigma^2}{2}\alpha f(\psi(t), t)\\ &+ \frac{\sigma^3}{6}\alpha\left(\frac{\partial f}{\partial\psi}(\psi(t+\theta\sigma), t+\theta\sigma)\dot{\psi}(t+\theta\sigma) + \frac{\partial f}{\partial t}(\psi(t+\theta\sigma), t+\theta\sigma)\right),\end{aligned} \tag{22}$$

with $0 < \theta < 1$. From expansion (22) we can derive the following estimator for the relative error at $t = t^{m+1}$:

$$E^{m+1} = \frac{\sigma^3}{6}\alpha\frac{\left|\frac{\partial f}{\partial\psi}(\frac{\psi^{m+1}+\psi^m}{2}, t^m)\frac{\psi^{m+1}-\psi^m}{\sigma}\right| + \left|\frac{\partial f}{\partial t}(\frac{\psi^{m+1}+\psi^m}{2}, t^m)\right|}{\max[1, |\psi^{m+1}|]}. \tag{23}$$

In order to adapt σ using E^{m+1}, we may proceed as follows: If ψ^{m+1} obtained from scheme (21) verifies

$$E^{m+1} \leq tol, \tag{24}$$

keep integrating with σ as time discretization step. If criterion (24) is not verified, we have two possible situations

a) $\underline{m = 0}$:
- Divide σ by 2 as many times it is necessary to have

$$E^1 \leq \frac{tol}{5}. \tag{25}$$

  Each time σ is divided by 2, double M accordingly.
- Still calling σ the first time-step for which (25) holds after successive divisions by 2, apply scheme (21) to the solution of (20), with the new σ and the associated M.

b) $\underline{m \geq 1}$:
- Go to $t = t^{m-1/2} = t_0 + (m - 1/2)\sigma$.
- $t^{m-1/2} \to t_0$, $\frac{\psi^{m-1}+\psi^m}{2} \to \psi_0$, $\frac{\psi^m - \psi^{m-1}}{\sigma} \to \psi_1$.
- $\sigma \to \sigma/2$.
- $2(M - m) + 1 \to M$.
- Apply scheme (21) on the new interval (t_0, t_f). If criterion (24) is not verified, then proceed as in a).

For the numerical results reported in Section 4, we used $tol = 10^{-4}$.

4. Numerical results. In this section, we are going to report on the results of numerical experiments concerning the solution of the nonlinear wave problem (6),(3),(4).

As mentioned in Section 1, we will take three different forcing terms in (6). In Section 4.1, we are reporting the results obtained when the nonlinear forcing term in (6) is the same as that of the Painlevé I equation; in Section 4.2, when it is given by the nonlinear forcing term of the Painlevé II equation; and in Section 4.3 when it is the exponential nonlinearity encountered in the Bratu problem.

For all the problems, we take $\Omega = (0,1)^2$.

4.1. Painlevé I. In this section, we consider the particular case of (6) where the nonlinear forcing term is borrowed from the Painlevé I equation, namely:

$$f(u,t) = 6u^2 + t. \tag{26}$$

The non-damped version of (6), i.e. with $k = 0$, with forcing term as in (26) has been studied in [1], for both Dirichlet boundary conditions (4) and mixed boundary Dirichlet-Sommerfel conditions (5). Here, we consider only condition (4) and aim at checking the effect of the damping term on the blow-up time.

For the numerical results presented below, we took:

- $u_0 = 0$ and $u_1 = 0$.
- c ranging from 0 to 1.5.
- $\alpha = \beta = 1/2$.
- $h = 1/100$.
- $\Delta t = 10^{-2}$ for $c \in [0, 0.6]$, $\Delta t = 8 \times 10^{-3}$ for $c = 0.7, 0.8$, $\Delta t = 5 \times 10^{-3}$ for $c = 0.9, 1, 1.25$, $\Delta t = 10^{-3}$ for $c = 1.5$.

We initialized with $M = 3$ (see Section 3.1) and then adapted M following the procedure described in Section 3.2. We considered only $h = 1/100$ because the numerical experiments reported in [1] showed that the results obtained for $h = 1/100$ and $h = 1/150$ match very accurately.

Fig. 1 reports the variation of the blow-up time of the approximated solution as a function of c for three values of k: $k = 0, 1, 10$. It is not surprising to observe that for small values of c the blow-up time increases significantly with k. However, for c sufficiently large, the influence of k on the blow-up time becomes negligible.

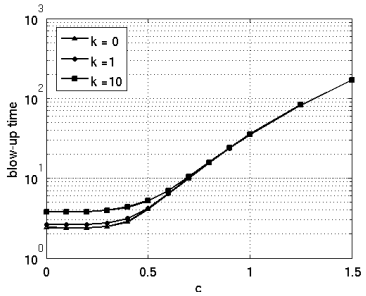

FIG. 1. *Painlevé I: Blow-up time as a function of c for $k = 0, 1, 10$ (semi-log scale).*

In Fig. 2, we show, for $c = 0.5$ and $k = 1$, the approximated evolution of the function

$$t \to \max_{\{x_1, x_2\} \in \Omega} u(x_1, x_2, t) \tag{27}$$

for different values of ϵ. The computed maximum value is always achieved at $\{0.5, 0.5\}$. From Fig. 2, we see that a difference in four orders of magnitude for ϵ has a little effect on the evolution of the function in (27).

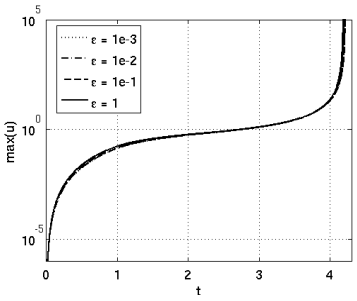

FIG. 2. *Painlevé I: Evolution of the computed approximation of the function in (27) for $c = 0.5$, $k = 1$, and different values of ϵ (semi-log scale).*

4.2. Painlevé II. We will now consider the case when the forcing term in (6) is the one encountered in the Painlevé II equation, namely:

$$f(u,t) = 2u^3 + tu + \gamma, \quad \gamma \in \mathbb{C}. \tag{28}$$

Let us write the complex constant γ in terms of its modulus and phase ϕ, that is $\gamma = |\gamma|\cos\phi + i|\gamma|\sin\phi$ and u in terms of its real part u_R and imaginary part u_I, that is $u = u_R + iu_I$. Then, the real and imaginary parts of equation (6) with forcing term as in (28) are given by:

$$\begin{cases} \dfrac{\partial^2 u_R}{\partial t^2} + \dfrac{k}{\epsilon + t}\dfrac{\partial u_R}{\partial t} - c^2\nabla^2 u_R = 2u_R^3 - 6u_I^2 u_R + tu_R + |\gamma|\cos\phi \quad \text{in } \Omega \in (0, T_{\max}), \\ \dfrac{\partial^2 u_I}{\partial t^2} + \dfrac{k}{\epsilon + t}\dfrac{\partial u_I}{\partial t} - c^2\nabla^2 u_I = -2u_I^3 + 6u_R^2 u_I + tu_I + |\gamma|\sin\phi \quad \text{in } \Omega \in (0, T_{\max}). \end{cases}$$

Notice that the above two equations are strongly (and nonlinearly) coupled.

In order to apply the procedure described in Section 3 for the treatment of the nonlinearity, we decided to estimate the relative error (23) as follows:

$$E^{m+1} = \frac{\sigma^3}{6}\alpha\frac{(6|\bar{u}^{m+1}|^2|\dot{u}^{m+1}| + |\bar{u}^{m+1}| + t^{m+1}|\dot{u}^{m+1}|)}{\max[1, |u^{m+1}|]},$$

with

$$|\bar{u}^{m+1}| = \left(\left(\frac{u_R^{m+1} + u_R^m}{2}\right)^2 + \left(\frac{u_I^{m+1} + u_I^m}{2}\right)^2\right)^{1/2},$$

$$|\dot{u}^{m+1}| = \left(\left(\frac{u_R^{m+1} - u_R^m}{\sigma}\right)^2 + \left(\frac{u_I^{m+1} - u_I^m}{\sigma}\right)^2\right)^{1/2}.$$

We take the same values for u_0, u_1, α, β, and h as in Section 4.1. First, we set $k = 0$, $c = 0.1$, $\Delta t = 10^{-2}$, $|\gamma| = 1$, and check how ϕ, i.e. the phase of γ, affects the blow-up time. We consider eight values for ϕ: $0, \frac{\pi}{6}, \frac{\pi}{4}, \frac{\pi}{3}, \frac{2\pi}{3}, \frac{3\pi}{4}, \frac{5\pi}{6}, \pi$. The

corresponding blow-up times are reported in Fig. 3. We see that the blow-up time increases for $\phi \in [0, \pi/2)$ and decreases for $\phi \in (\pi/2, \pi]$. As for $\phi = \pi/2$, we display in Fig. 4(a) the approximated evolution of the function

$$t \to \max_{\{x,1,x_2\}\in\Omega} u_I(x_1, x_2, t). \tag{29}$$

Fig. 4(a) indicates that for $\phi = \pi/2$ the solution u, that has $u_R \equiv 0$, does not blow-up for $t \in (0, 1000)$. Fig. 4(b) shows a zoomed view of Fig. 4(a). Fig. 4(a) suggests that the blow-up does not occur in finite time, but only asymptotically as $t \to +\infty$.

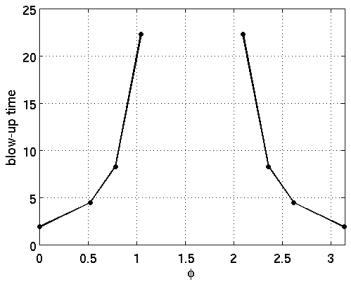

FIG. 3. *Painlevé II: Blow-up time as a function of ϕ for $c = 0.1$, $k = 0$, $|\gamma| = 1$.*

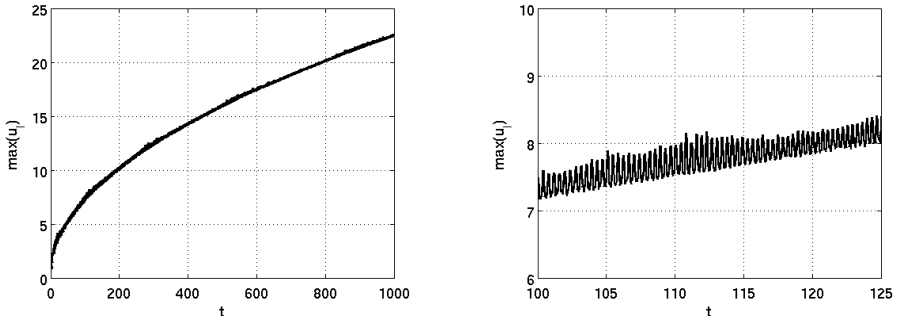

(a) function (29) (b) zoomed view of (a)

FIG. 4. *Painlevé II: (a) Computed approximation of the function in (29) for $\phi = \dfrac{\pi}{2}$, $|\gamma| = 1$, $c = 0.1$, $k = 0$ and (b) Zoomed view of (a).*

In Fig. 5 and 6, we show the modulus and phase of the computed approximation of u for $k = 0$, $c = 0.1$, $|\gamma| = 1$ and $\phi = \dfrac{\pi}{6}, \dfrac{\pi}{4}, \dfrac{\pi}{3}, \dfrac{2\pi}{3}, \dfrac{3\pi}{4}, \dfrac{5\pi}{6}$ at a time just before blow-up. The computed solutions for the pairs $\left\{\dfrac{\pi}{6}, \dfrac{5\pi}{6}\right\}$, $\left\{\dfrac{\pi}{4}, \dfrac{3\pi}{4}\right\}$, $\left\{\dfrac{\pi}{3}, \dfrac{2\pi}{3}\right\}$ have the same modulus and opposite phase before blow-up.

Next, we let c and k vary and check the effect on the blow-up time and the solution very close to explosion. Fig. 7 reports the blow-up time as a function of $c \in [0.1, 0.6]$ for two values of ϕ and different values of k. For all the values of c, Δt was set to 10^{-2}. From Fig. 7, we see that if γ is a real constant, i.e. $\phi = 0$, the blow-up time increases with c, as it happens when the forcing term in (6) is given

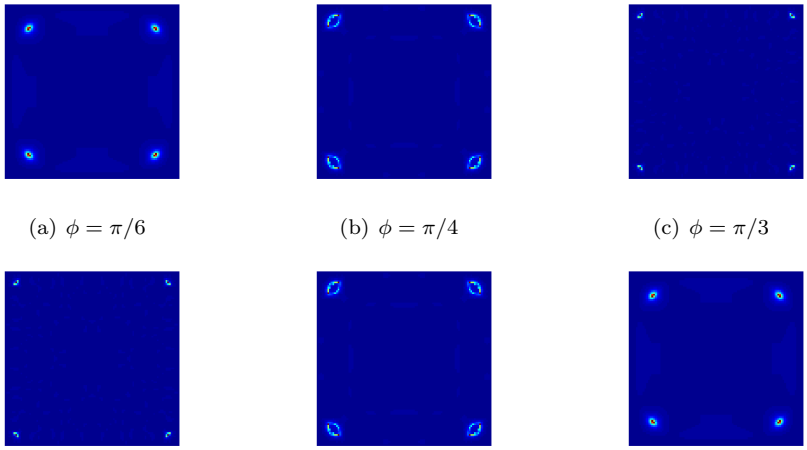

(a) $\phi = \pi/6$ (b) $\phi = \pi/4$ (c) $\phi = \pi/3$

(d) $\phi = 2\pi/3$ (e) $\phi = 3\pi/4$ (f) $\phi = 5\pi/6$

FIG. 5. *Painlevé II: Modulus of the solution close to explosion for* $c = 0.1$, $k = 0$, $|\gamma| = 1$, *and different phases of* γ. *Blue corresponds to 0 and red to 300. (Please refer to the online version of the article for colors.)*

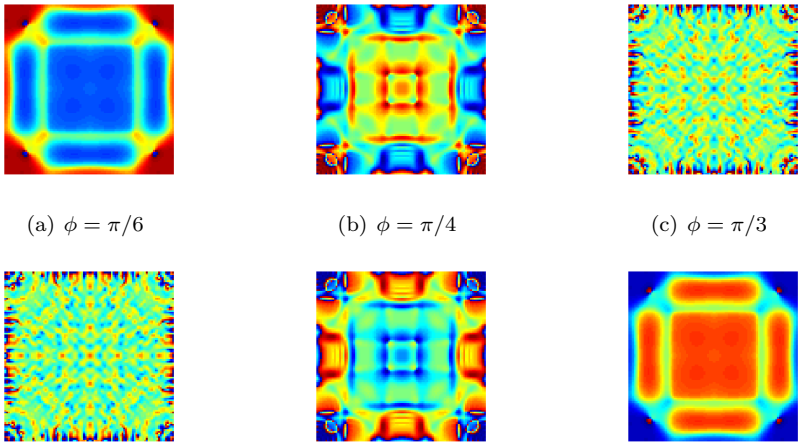

(a) $\phi = \pi/6$ (b) $\phi = \pi/4$ (c) $\phi = \pi/3$

(d) $\phi = 2\pi/3$ (e) $\phi = 3\pi/4$ (f) $\phi = 5\pi/6$

FIG. 6. *Painlevé II: Phase of the solution close to explosion for* $c = 0.1$, $k = 0$, $|\gamma| = 1$, *and different phases of* γ. *Blue corresponds to* $-\pi/2$ *and red to* $\pi/2$. *(Please refer to the online version of the article for colors.)*

by the one in (26). Also, as with the nonlinearity in (26), for small values of c the blow-up time increases significantly with k, and for c sufficiently large the influence of k is negligible. However, when the imaginary part of γ is different from 0 (as it is for the case in Fig. 7, which corresponds to setting $\phi = \pi/6$), things are very different: the blow-up time is no more an increasing function of c and a larger value of k does

not cause a larger blow-up time. For $\phi = \pi/6$, both $k = 0$ and $k = 1$, the blow-time seems to oscillate as c varies. The curve for $k = 10, \phi = \pi/6$ is missing in Fig. 7 because no blow-up is observed over for $t \in (0, 1000)$: regardless of the value of c, the modulus of the computed solution displays an oscillatory behavior similar to the graph in Fig. 4(a), that is the norm of the solution increases in time but the blow-up occurs in an infinite time rather than at a finite time as for $k = 0, 1$.

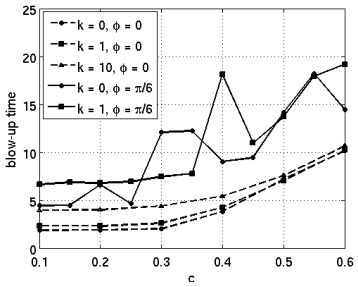

FIG. 7. *Painlevé II: Blow-up time as a function of c for* $|\gamma| = 1$, $\phi = 0, \pi/6$, *and different values of* k.

In Fig. 8 and 9, we show the modulus and phase of the computed approximation of u for $k = 0$, $|\gamma| = 1$, $\phi = \pi/6$ and $c = 0.1, 0.2, 0.3, 0.4, 0.5, 0.6$ at a time very close to explosion. Notice how modulus and phase change significantly from $c = 0.1$ to $c = 0.2$ but then remain practically unchanged for higher values of c. We repeat the same numerical experiments but set $k = 1$. Modulus and phase of the computed approximation of u are reported in Fig. 10 and 11, respectively. For $k = 1$, the modulus and phase of the solution do not vary much till $c = 0.3$ and then rapidly change to form different patterns.

A natural variation of the above model with physical relevance is to replace the cubic term in (28) by the following *Ginzburg-Landau* type nonlinearity (see [7] for related physical applications):

$$f(u,t) = 2|u|^2 u + tu + \gamma, \quad \gamma \in \mathbb{C}. \tag{30}$$

The real and imaginary parts of equation (6) with forcing term as in (30) are given by:

$$\begin{cases} \dfrac{\partial^2 u_R}{\partial t^2} + \dfrac{k}{\epsilon + t}\dfrac{\partial u_R}{\partial t} - c^2\nabla^2 u_R = 2u_R^3 + 2u_I^2 u_R + tu_R + |\gamma|\cos\phi \quad \text{in } \Omega \in (0, T_{\max}), \\ \dfrac{\partial^2 u_I}{\partial t^2} + \dfrac{k}{\epsilon + t}\dfrac{\partial u_I}{\partial t} - c^2\nabla^2 u_I = 2u_I^3 + 2u_R^2 u_I + tu_I + |\gamma|\sin\phi \quad \text{in } \Omega \in (0, T_{\max}). \end{cases}$$

We solved the above problem for $k = 10$ and $\phi = \pi/6$, that is the values of k and ϕ for which we observed no explosion for (6),(28). The approximated solution to (6),(30) does blow up in this case and in Fig. 12, we show the blow-up time as a function of $c \in [0.1, 0.6]$. For all c, the modulus of the solution at a time very close to explosion looks like the solution to (6),(26) or (6),(28) with $\gamma \in \mathbb{R}$, that is a high peak at $\{x_1, x_2\} = \{0.5, 0.5\}$, while the phase is equal to $\pi/3$ everywhere inside Ω.

4.3. Bratu. Finally, we consider the case where the nonlinearity of the forcing term in (6) is given by:

$$f(u) = \lambda e^u, \quad \lambda \in \mathbb{R}^+, \tag{31}$$

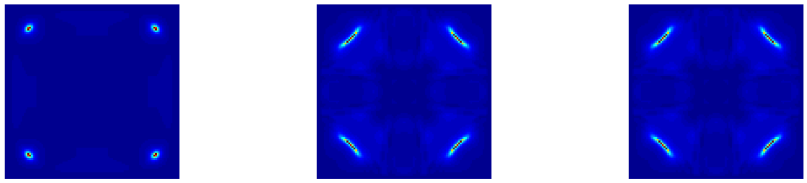

(a) $c = 0.1$ (b) $c = 0.2$ (c) $c = 0.3$

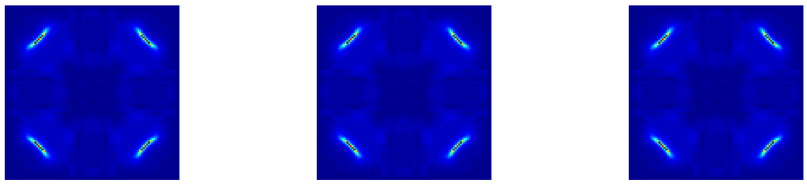

(d) $c = 0.4$ (e) $c = 0.5$ (f) $c = 0.6$

FIG. 8. *Painlevé II: Modulus of the solution close to explosion for* $k = 0$, $|\gamma| = 1$, $\phi = \pi/6$, *and different values of* c. *Blue corresponds to 0 and red to 300. (Please refer to the online version of the article for colors.)*

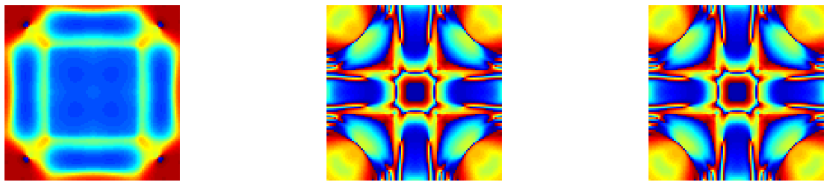

(a) $c = 0.1$ (b) $c = 0.2$ (c) $c = 0.3$

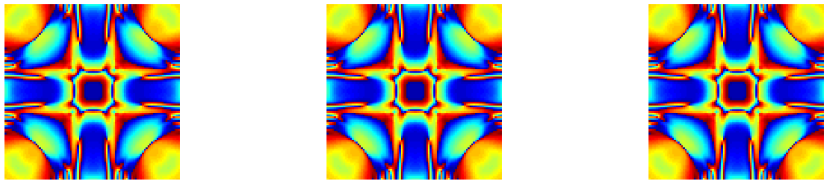

(d) $c = 0.4$ (e) $c = 0.5$ (f) $c = 0.6$

FIG. 9. *Painlevé II: Phase of the solution close to explosion for* $k = 0$, $|\gamma| = 1$, $\phi = \pi/6$, *and different values of* c. *Blue corresponds to* $-\pi/2$ *and red to* $\pi/2$. *(Please refer to the online version of the article for colors.)*

that is the celebrated *Bratu problem* nonlinearity (see, e.g., [8] for applications to solid combustion). Notice that this forcing term does not depend on t explicitly, unlike (26) and (28).

In order to apply the procedure described in Section 3 for the treatment of the

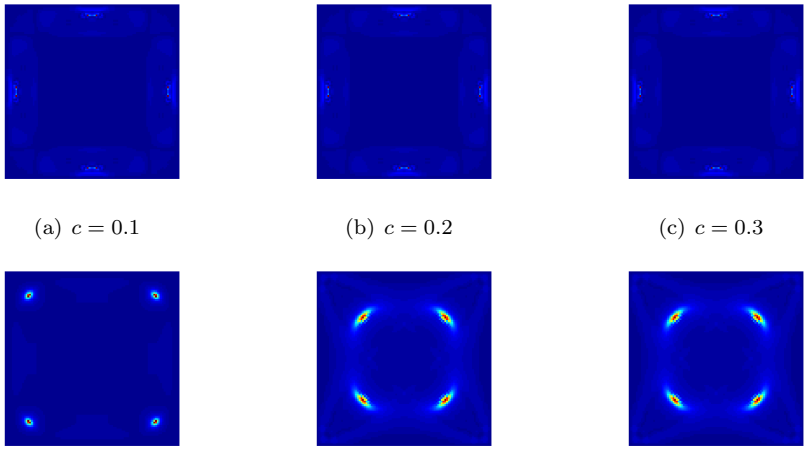

(a) $c = 0.1$ (b) $c = 0.2$ (c) $c = 0.3$

(d) $c = 0.4$ (e) $c = 0.5$ (f) $c = 0.6$

FIG. 10. *Painlevé II: Modulus of the solution close to explosion for $k = 1$, $|\gamma| = 1$, $\phi = \pi/6$, and different values of c. Blue corresponds to 0 and red to 300. (Please refer to the online version of the article for colors.)*

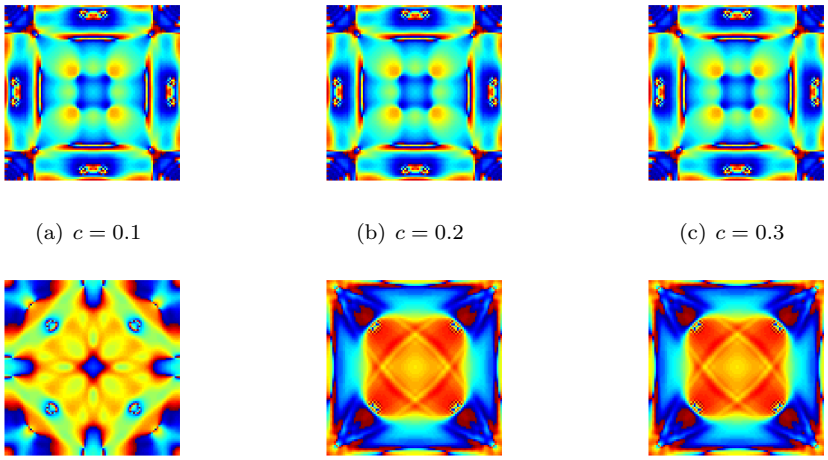

(a) $c = 0.1$ (b) $c = 0.2$ (c) $c = 0.3$

(d) $c = 0.4$ (e) $c = 0.5$ (f) $c = 0.6$

FIG. 11. *Painlevé II: Phase of the solution close to explosion for $k = 1$, $|\gamma| = 1$, $\phi = \pi/6$, and different values of c. Blue corresponds to $-\pi/2$ and red to $\pi/2$. (Please refer to the online version of the article for colors.)*

nonlinearity, we estimate the relative error (23) as follows:

$$E^{m+1} = \frac{\sigma^3}{6}\alpha\lambda \frac{e^{\frac{u^{m+1}+u^m}{2}}\left|\dfrac{u^{m+1}-u^m}{\sigma}\right|}{\max[1,|u^{m+1}|]},$$

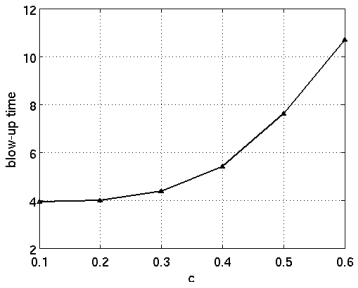

FIG. 12. *Ginzburg-Landau: Blow-up time as a function of c for* $|\gamma| = 1$, $\phi = \pi/6$, $k = 10$.

We take the same values for u_0, u_1, α, β, and h as in Section 4.1. Moreover, let us start by setting $k = 0$ in (6) and $\lambda = 1$ in (31). For c small enough, we observe the same explosive nature of the solution that we have seen for (26) and (28); see Table 1 for the blow-up times. For $c = 0.32$, Fig. 13 reports the evolution of the computed approximation of the function in (27) for $t \in [0, 2.94]$ and the computed approximation for $p = \dfrac{\partial u}{\partial t}$ at $t = 2.94$ (very close to blow-up).

TABLE 1
Bratu, $k = 0$*: Blow-up times for different values of c.*

	c = 0.1	c = 0.2	c =0.3	c=0.31	c=0.32	c=0.33
blow-up time	1.99	1.99	2.48	2.66	2.94	3.72

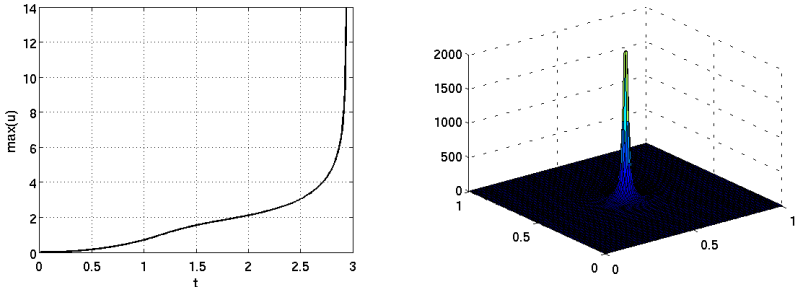

(a) the function in (27) (b) p at $t = 2.94$

FIG. 13. *Bratu,* $\lambda = 1$, $k = 0$, $c = 0.32$*: (a) Evolution of the computed approximation of the function in (27) for* $t \in [0, 2.94]$ *and (b) Computed approximation of p at* $t = 2.94$.

For c above a critical value c_{cr}, the solution to (6),(31) does not blow-up anymore. For $k = 0$ and $\lambda = 1$, the numerical results suggest that $0.33 < c_{cr} < 0.34$. In Fig. 14(a), we show the evolution of the computed approximation of the function in (27) for $c = 0.34$. Figure 14(b) suggests that the modulation for $c = 0.34$ observed in Fig. 14(a) is quasi-monochromatic signal, with $f \simeq 0.22$ Hz. It is possible to get a good estimate of the critical value c_{cr} by considering the static version of the equation

under consideration, that is:

$$\begin{cases} -\nabla^2 u = \dfrac{\lambda}{c^2} e^u & \text{in } \Omega, \\ \\ u = 0 & \text{on } \partial\Omega. \end{cases}$$

It is well known that the above problem possesses a *turning point* for $\dfrac{\lambda}{c^2} \simeq 6.81$ (see, e.g., [9], Chapter 3). This means that c_{cr} can be estimated by $c_{cr} \simeq \sqrt{\lambda/6.81}$. So, for $\lambda = 1$ we get $c_{cr} \simeq 0.38$, which is not too far from the value suggested by the numerical experiments.

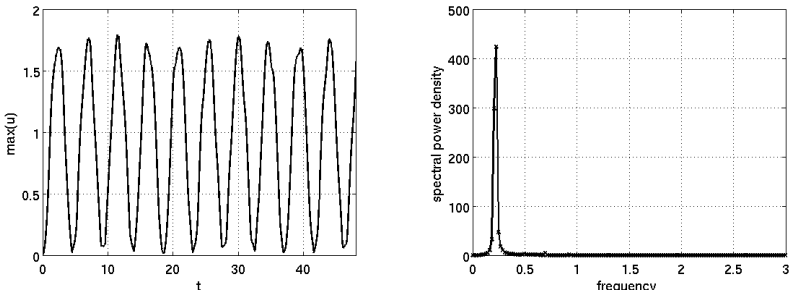

(a) the function in (27) (b) spectral power density for (a)

FIG. 14. *Bratu, $\lambda = 1$, $k = 0$, $c = 0.34$: (a) Evolution of the computed approximation of the function in (27) and (b) Spectrum of the modulation.*

If we solve problem (6),(31) with $k = 0$, $\lambda = 1$, and $c = 0.4$, the oscillations of the function in (27) have smaller amplitude and higher frequency than for $c = 0.34$, which is closer to c_{cr}. See Fig. 15. Again, the spectral power density (in Fig. 15(b)) suggests that the modulation of function (27) in Fig. 15(a) is a quasi-monochromatic signal, with $f \simeq 0.32$ Hz in this case.

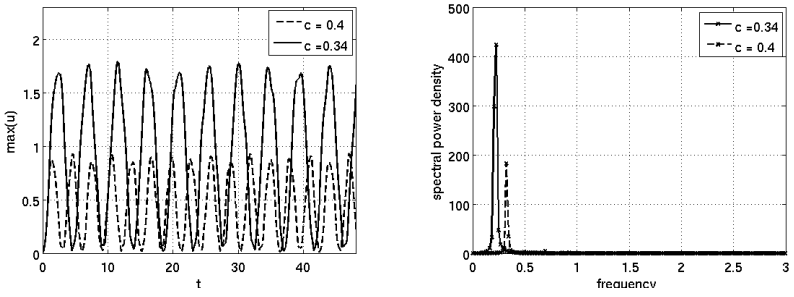

(a) the function in (27) (b) spectral power density for (a)

FIG. 15. *Bratu, $\lambda = 1$, $k = 0$: Comparison between $c = 0.34$ and $c = 0.4$ in terms of (a) Evolution of the computed approximation of the function in (27) and (b) Spectrum of the modulation.*

Next, let us set $k = 1$, while keeping $\lambda = 1$. As for $k = 0$, for small values of c the solution to (6),(31) displays an explosive nature. See Table 3 for the blow-up times, which are higher than in the non-damped case (compare with the times in Table 1).

Also, a higher k has the effect of reducing the value of c_{cr}: the numerical results suggest that for $k = 1$ we have $0.31 < c_{cr} < 0.32$.

TABLE 2
Bratu, $\lambda = 1$, $k = 1$: Blow-up times for different values of c.

	c = 0.1	c = 0.2	c =0.3	0.31
blow-up time	2.52	2.57	3.82	4.63

In Figure 16(a), we show the evolution of the computed approximation of the function in (27) for $c = 0.32$ and $c = 0.4$. Fig. 16(b) reports the spectrum of the modulations in 16(a): the damped oscillations of the function in (27) have frequency $f \simeq 0.18$ Hz for $c = 0.32$ and $f \simeq 0.33$ Hz for $c = 0.4$. Notice that the effective damping coefficient in (6) is $k/(\epsilon + t)$, so as $t \to \infty$ it approaches zero. We let the simulations whose results are reported in Fig. 16 run till $t = 1000$. For $c = 0.32$ (resp., 0.4) the amplitude of the oscillations is 0.12 (resp., 0.035) at $t = 200$ and 0.055 (resp., 0.016) at $t = 1000$.

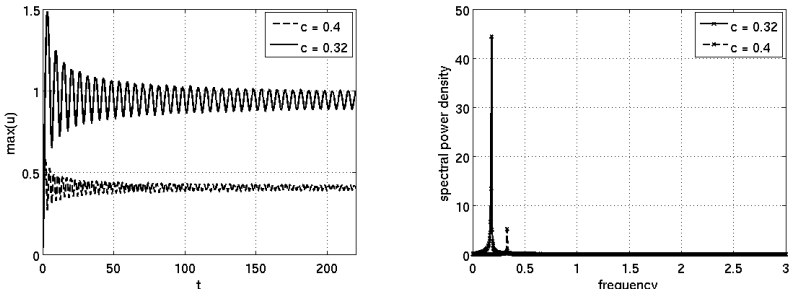

(a) the function in (27) (b) spectral power density for (a)

FIG. 16. *Bratu, $\lambda = 1$, $k = 1$: Comparison between $c = 0.32$ and $c = 0.4$ in terms of (a) Evolution of the computed approximation of the function in (27) and (b) Spectrum of the modulation.*

Next, we set $k = 10$, while keeping $\lambda = 1$. The value of c_{cr} is further reduced: the numerical results suggest that we have $0.3 < c_{cr} < 0.31$. See Table 3 for the blow-up times for $c = 0.1, 0.2, 0.3$. In Figure 17(a), we show the evolution of the computed approximation of the function in (27) for $c = 0.31$ and $c = 0.4$. Unlike the cases $k = 0$ and $k = 1$, the function in (27) does not display an oscillatory behavior. The computed solution u approaches a steady state (which is clearly the solution of the associated steady Bratu's problem) after the initial transitory phase. Figure 17(b) shows the computed approximation of u at $t = 70$ (close to the steady state) for $c = 0.4$.

TABLE 3
Bratu, $\lambda = 1$, $k = 10$: Blow-up times for different values of c.

	c = 0.1	c = 0.2	c =0.3
blow-up time	4.85	5.22	10.02

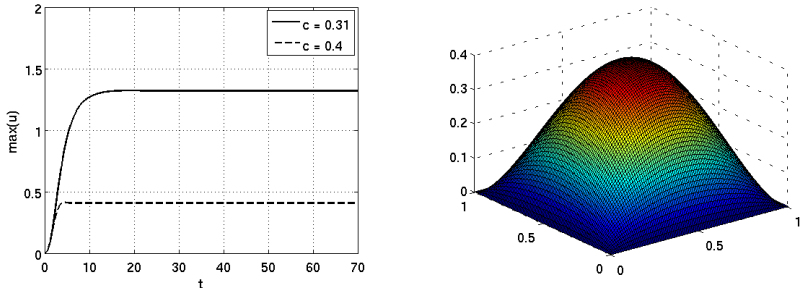

(a) the function in (27) (b) u at $t = 70$ for $c = 0.4$

FIG. 17. *Bratu, $\lambda = 1$, $k = 10$: (a) Comparison between $c = 0.31$ and $c = 0.4$ in terms of evolution of the computed approximation of the function in (27) and (b) Computed approximation of u at $t = 70$ for $c = 0.4$.*

Fig. 16(a) and 17(a) suggest that there is a critical value of k between 1 and 10 at which the oscillatory behavior of the function in (27) disappears. To estimate such a value, we fixed $\lambda = 1$, $c = 0.4$, and progressively increased the value of k. For $k = 2$, the function in (27) is still oscillating at $t = 1000$ with amplitude $5 \cdot 10^{-4}$. For $k = 3$, amplitude $5 \cdot 10^{-4}$ is already reached at $t = 100$, while at $t = 1000$ the amplitude is $2 \cdot 10^{-5}$. For $k = 8$, at $t = 50$ the amplitude of the oscillations is 10^{-6}, whereas for $k = 9$ there are no oscillations. Thus, the critical value of k is between 8 and 9.

Fig. 18 is a zoom of Fig. 15(a), 16(a), and 17(a), that is it shows the evolution of the computed approximation of the function in (27) for $k = 0, 1, 10$ over the interval $[0, 2]$, when the damping coefficient $k/(\epsilon + t)$ is large.

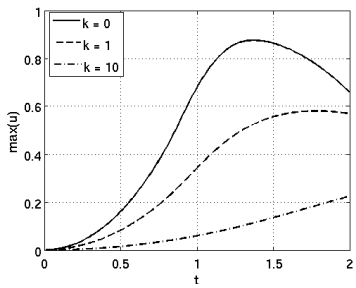

FIG. 18. *Bratu, $\lambda = 1$, $c = 0.4$: evolution of the computed approximation of the function in (27) for $k = 0, 1, 10$ over the interval $[0, 2]$. This figure is a zoom of the corresponding curves in Fig. 15(a), 16(a), and 17(a).*

Finally, we replaced the time dependent damping coefficient $k/(\epsilon + t)$ by k to check how the solution u varies. So, instead of (6), we now consider

$$\frac{\partial^2 u}{\partial t^2} + k\frac{\partial u}{\partial t} - c^2\nabla^2 u = f(u,t) \quad \text{in } \Omega \in (0, T_{\max}). \tag{32}$$

Problem (32) can be easily solved using a three-stage operator-splitting scheme of the Strang's type; however, for commonality we still used a five-stage operator-splitting scheme, namely, the one obtained by replacing $k/(\epsilon + t^{n+1/2})$ by k in (15) and (17). Therefore, steps 1, 3, and 5 are still given by (14), (16), and (18), while step 2 becomes:

Set $u^{n+2/5} = u^{n+1/5}$, $p^{n+2/5} = p\left(\frac{\Delta t}{2}\right)$, p being the solution of

$$\begin{cases} \dfrac{\partial p}{\partial t} + kp = 0 \text{ in } \Omega \times \left(0, \dfrac{\Delta t}{2}\right), \\ \\ p(0) = p^{n+1/5}; \end{cases} \tag{33}$$

and step 4 becomes: Set $u^{n+4/5} = u^{n+3/5}$, $p^{n+4/5} = p\,(\Delta t)$, p being the solution of

$$\begin{cases} \dfrac{\partial p}{\partial t} + kp = 0 \text{ in } \Omega \times \left(\dfrac{\Delta t}{2}, \Delta t\right), \\ \\ p\left(\dfrac{\Delta t}{2}\right) = p^{n+3/5}. \end{cases} \tag{34}$$

The solutions to sub-problems (33) and (34) are given by:

$$p^{n+2/5} = e^{-\frac{k\Delta t}{2}} p^{n+1/5}, \quad p^{n+4/5} = e^{-\frac{k\Delta t}{2}} p^{n+3/5}, \tag{35}$$

respectively.

In Figure 19, we show the evolution of the computed approximation of the function in (27) for $c = 0.4$ and $k = 1$. Since the damping coefficient is constant, the oscillations are damped out quickly (compare Fig. 19 with the the dashed line in Fig. 16(a)).

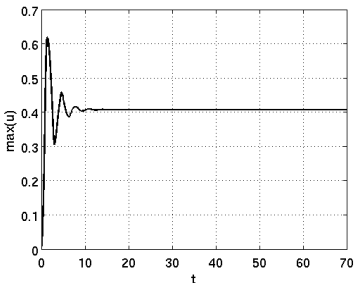

FIG. 19. *Evolution of the computed approximation of the function in (27) where u is the solution to (32)-(31) for* $\lambda = 1$, $c = 0.4$, *and* $k = 1$.

5. Conclusion. In this article, we have investigated the numerical solution of nonlinear wave equations of the Euler-Poisson-Darboux type. Various nonlinear forcing terms have been considered, including a complex-valued one. Depending on the respective values of the various parameters in the model and on the nonlinearity, solutions can blow-up in finite time or evolve to a limit cycle. The key ingredient to capture the solutions has been a five-stage symmetrized splitting scheme for the time discretization coupled to a well-chosen time-step adaptation technique for treating the fractional steps associated with the nonlinear forcing term of the equation.

Acknowledgements. The authors would like to thank the founders of the *Painlevé Project*; their initiative is at the origin of this work.

REFERENCES

[1] R. Glowinski and A. Quaini, *On the numerical solution of a nonlinear wave equation associated with the first Painlevé equation: An operator-splitting approach*, Chinese Annals of Mathematics, Series B, 34:2 (2013), pp. 237–254.

[2] G. Strang, *On the construction and comparison of difference schemes*, SIAM J. Numer. Anal., 5:3 (1968), pp. 506–517.

[3] J. B. Keller, *On solutions of nonlinear wave equations*, Comm. Pure Appl. Math., 10:4 (1957), pp. 523–530.

[4] R. Glowinski, L. Shiau, and M. Sheppard, *Numerical methods for a class of nonlinear integro-differential equations*, Calcolo, 50:1 (2013), pp. 17–33.

[5] A. M. Genis, *On finite element methods for the Euler-Poisson-Darboux equation*, SIAM J. Numer. Anal., 12:6 (1984), pp. 1080–1106.

[6] A. A. Samarski, V. A. Galaktionov, S. .P. Kurdyumov, and A. P. Mikhailov, *Blow-up in quasilinear parabolic equations*, de Gruyter Expositions in Mathematics, vol. 19, de Gruyter, Berlin and Hawthorne, NY, 1995.

[7] M. J. Landman, G. C. Papanicolaou, C. Sulem, P. L. Sulem, and X. P. Wang, *Stability of isotropic singularities for the nonlinear Schrödinger equation*, Physica D, 47 (1991), pp. 393–415.

[8] J. Bebernes, and D. Eberly, *Mathematical Problems from Combustion Theory*, Springer-Verlag, New York, NY, 1989.

[9] R. Glowinski, *Finite Element Methods for Incompressible Viscous Flow*, in "Handbook of Numerical Analysis", Vol. IX, P. G. Ciarlet & J. L. Lions, eds., North-Holland, Amsterdam, 2003, pp. 3–1176.